Experiments Using a 25-kw Hollow Cathode Lithium Vapor MPD Arcjet

D. B. Fradkin,* A. W. Blackstock,* D. J. Roehling,*
T. F. Stratton,* M. Williams,† and K. W. Liewer‡
Los Alamos Scientific Laboratory, Los Alamos, N. Mex.

The performance is reported of a 25-kw, lithium fueled, applied field MPD arcjet which incorporates a unique feed system with an "open-ended heat-pipe" vaporizer and a hollow cathode. The arc typically operates at currents of 250–500 amp, voltages of 40–60 v, magnetic field strengths between 500 and 3000 gauss, and produces a highly ionized lithium beam which transports 70% of the input electrical power to the beam stop. The ambient tank pressures range as low as 2×10^{-7} torr. A comparison of hollow cathode and conventional MPD arc performance is made and it is concluded that the hollow cathode arc is superior to the conventional design. Diagnostic experiments performed in the exhaust plume include the determination of axial ion and atom velocities by measurements of Doppler shifts with a scanning Fabry-Perot interferometer and of ion energies by use of electrostatic energy analyzers; the determination of ion temperatures by comparison of experimental and calculated spectral line profiles; the determination of electron temperatures and densities with electrostatic probes; and the determination of current densities by Rogowski loops. These measurements indicate that at a station 25 cm downstream of the arc head the directed ion velocity exceeds 2×10^6 cm/sec. At a station 90 cm downstream the plasma typically has an electron temperature of about 2.3 ev, a density of approximately 1.5×10^{12} cm^{-3}, and under certain operating conditions more than 40% of the arc current extends 90-cm downstream of the arc head. The efficiency of a process that converts input electrical power into kinetic energy is discussed in terms of a model which sets the plasma into rotation with subsequent expansion in a magnetic field.

I. Introduction

PLASMA accelerators that generate a plasma by the discharge of electrical current between short coaxial electrodes in the presence of an applied axially symmetric magnetic field, and which are commonly called magnetoplasmadynamic, MPD, arcjets have been studied for space propulsion applications in a number of laboratories.[1–10] Despite the concerted effort that has been made to understand MPD arc performance, the thrust production mechanisms are poorly understood, as indicated by the many conflicting assumptions, approximations, and processes that have been proposed.[11] Experimental results indicate that not all MPD devices appear to operate in the same manner. Nevertheless, the MPD arc still holds great promise as a primary spacecraft propulsion system for deep space exploration.

This paper describes a nominal 25-kw lithium, hollow cathode MPD arc thruster that generates a reproducible and steady, highly ionized lithium plasma beam. Lithium is chosen as the propellant to be investigated since it can be stored easily during long space missions, and it offers the promise of high frozen flow efficiencies due to its low first ionization and high second ionization potential. In addition, the "self pumping" effect of the condensable lithium allows laboratory testing at low tank pressures, typically 2×10^{-7} torr for our test facility.

Received February 13, 1969; presented as Paper 69–241 at the AIAA 7th Electric Propulsion Conference, Williamsburg, Va., March 3–5, 1969; revision received July 12, 1969. Work performed under the auspices of the U.S. Atomic Energy Commission. The authors wish to acknowledge the many helpful discussions with G. Grover, and the contributions of R. Wicklin in the design, fabrication, maintenance, and operation of the experimental equipment.

* Staff Member. Member AIAA.
† Staff Member.
‡ Summer Student.

II. Apparatus

Arc Structure

The arc structure was mounted horizontally in the end of a 0.9-m-diam by 1.5-m-long stainless steel vacuum chamber. The system is shown schematically in Fig. 1. The outer electrode or anode consisted of an annular tantalum radiator, niobium brazed to a tantalum cylinder. The anode was 3.75 cm i.d., 3.9 cm long and 9.1 cm o.d. at the radiator. The anode was press fitted into a tapered annular, water cooled stainless steel shell supported by the cooling tubes. The radiator temperature varied from 1000–2000°C dependent on arc power and propellant mass flow.

The cathode was a hollow tungsten tube 1.1 cm i.d., 1.9 cm o.d., and 3.7 cm long. The cathode was brazed into the end of the vaporizer section and into a tantalum support structure which provides a thermal gradient to the water cooled stainless steel holder. The use of the hollow cathode resulted in a very stable discharge originating inside the cathode tube. This stability allowed the complete removal of insulators from the arc region. The absence of insulators near the electrodes eliminated the serious problems of insulator cracking and erosion usually present in alkali metal fed arcs.

The lithium feed system consisted of a storage reservoir, a positive displacement bellows type piston and a lithium vaporizer. The piston was actuated by a d.c. motor with a tachometer speed regulation of better than $\frac{1}{2}$% under load.

Lithium Vaporizer

The piston outlet fed lithium through a stainless-steel tube into the vaporizer section (Fig. 2). The operation of the vaporizer is similar to that of a "heat pipe" and is as follows[12]: lithium enters the tube at the porous plug location and fills the wick structure by capillary action. Vaporization takes place along the entire wick structure which operates at ap-

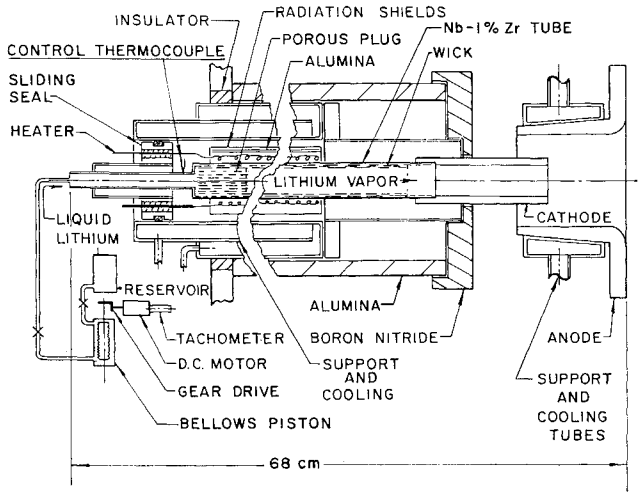

Fig. 1 Schematic of hollow cathode arc and lithium feed system.

proximately 1000°C, and fills the central volume with vapor which is forced out through the hollow cathode into the arc region. The feed rate is determined by the input power to the vaporizer heater. A control thermocouple is located in the region of the porous plug, sensing the temperature at a position upstream of the liquid-vapor interface. The signal from this thermocouple is fed into an integrating circuit that determines the difference between the signal and a predetermined set point. This circuit then controls the d.c. motor at the speed necessary to maintain the temperature of the control thermocouple at the set point. The actual lithium feed rate is then given independently by both the tachometer reading and by the input power to the vaporizer heater. These two quantities were found to agree to better than 5% during experimental runs. Arc startup was achieved by manual control of the feed system.

III. Arc Performance

The determination of the cathode operating characteristics and measurements of the gross arc operating characteristics of arc voltage and arc efficiency as a function of arc current, applied magnetic field strength, and input lithium mass flow, were deemed important for two reasons. Firstly, they would indicate whether the hollow cathode concept was promising for use in high power MPD arcs, and, secondly, they would indicate if there existed any major differences between the acceleration mechanisms of conventional and hollow cathode arcs.

Arc Voltage

The arc impedance was found to be smaller with larger current, larger with larger axial magnetic field strength, and

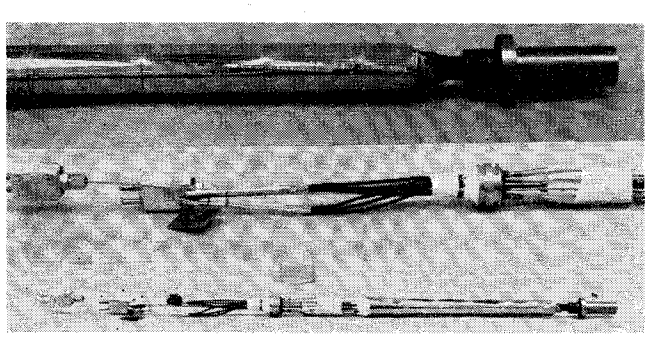

Fig. 2 Lithium vaporizer. Top: cathode end with radiation shields. Center: sliding seal. Bottom: complete assembly.

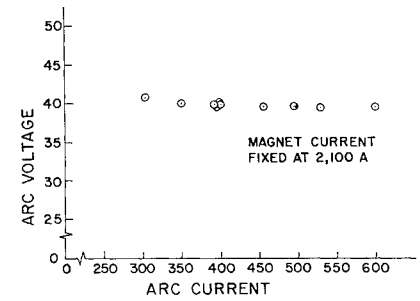

Fig. 3 Arc voltage vs arc current for hollow cathode arc at fixed magnetic field strength; magnetic field at anode face ≈ 0.485 gauss/amp.

virtually independent of the input mass flow when the input mass of lithium exceeded 15 mg/sec. Figures 3 and 4 show that for feed rates greater than 15 mg/sec the arc voltage is independent of the arc current and of input mass flow at fixed magnetic field strength. Similar results were obtained using a conventional arc. The arc voltage as a function of current in the axial magnetic field coils is plotted in Fig. 5. It is shown that points obtained at input mass flows greater than 15 mg/sec fall along a straight line described by the equation

$$V = V_o + U_c BR \tag{1}$$

where V_o is an additive constant to account for sheath and ohmic voltage drops, R is the anode radius, B the magnetic field strength near but somewhat downstream of the anode, and U_c the critical velocity of Alfvén.[13] This result was also obtained for several working fluids by Patrick and Schneiderman[5] and was discussed in Refs. 10 and 14 in terms of a model in which the dominant thrust producing mechanism was the conversion of rotational energy produced by $j_r B_z$ interactions into beam kinetic energy through expansion in a magnetic nozzle. At feeds below 15 mg/sec it was found that the arc jumped into a "high-voltage" mode of operation, a result also obtained in conventional lithium arcs.[14]

Thermal Efficiency

A comparison of the thermal efficiency, defined as the ratio of the total power in the beam to the total electrical input power to the arc, as a function of the applied magnetic field strength, is shown in Fig. 6. The power in the beam was determined from measurements of the flow rate and temperature rise of the coolant flowing through the vacuum chamber walls. Calorimetry was also performed on the electrode coolant. For all the reported points the sum of the electrode power and beam power agreed with the total electrical input power to the arc within 5%. The heat input to the hollow cathode was found to be very small, less than 3% of the electrical input power. Hollow cathode arc structures which did not incorporate a heater to vaporize the lithium would not run at low vacuum conditions since the heat input to the cathode was insufficient to vaporize an adequate amount of lithium. The heat inputs to the anode were similar for both conventional and hollow cathode arcs.

Beam Appearance

The hollow cathode arc was capable of producing an extremely steady and reproducible lithium plasma beam. At

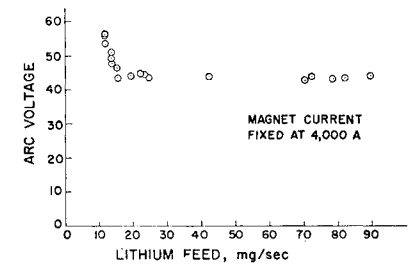

Fig. 4 Arc voltage vs input lithium feed rate for hollow cathode arc at fixed magnetic field strength; magnetic field at anode face ≈ 0.275 gauss/amp.

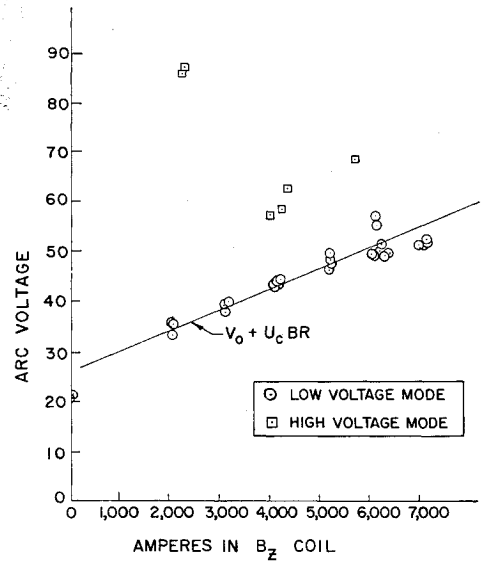

Fig. 5 Arc voltage vs current in magnetic field coils for hollow cathode arc; magnetic field at anode face ≈ 0.275 gauss/amp.

high-input mass flow rates the beam was a bright red, indicating a high proportion of neutrals. As the feed rate was lowered and the arc operated in the "high-voltage" mode the beam became almost transparent with a faint violet tinge as was the case for the conventional arc.[14] Figure 7 shows a photograph of the ionized lithium beam taken through a 5485 Å interference filter. The beam appears to follow the magnetic flux tube originating at the anode i.d. The light emitted by the ionized portion of the beam as viewed through the filter was more intense when the arc operated in the high voltage mode.

Cathode Operation

The hollow cathode was found to be superior to the conventional cathode in several respects. The current and voltage fluctuations were much smaller with the hollow cathode arc. Typical current fluctuations were less than five amp from the set current level. The hollow cathode was much more rugged than the conventional cathode. It was found that the hollow cathode was not damaged by operation in the

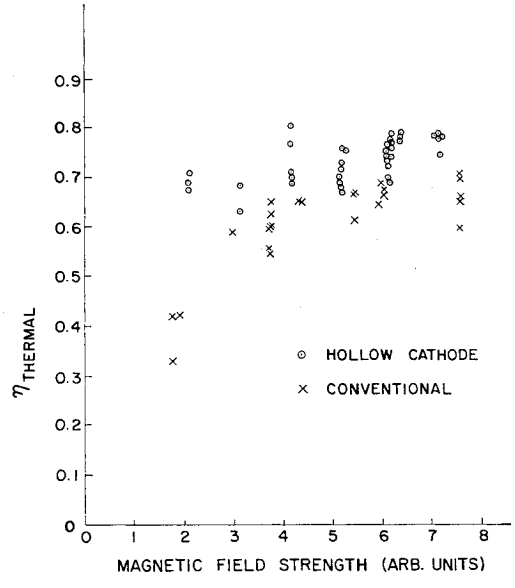

Fig. 6 Thermal efficiency vs current in magnetic field coils; magnetic field at anode face ≈275 gauss/abscissa unit.

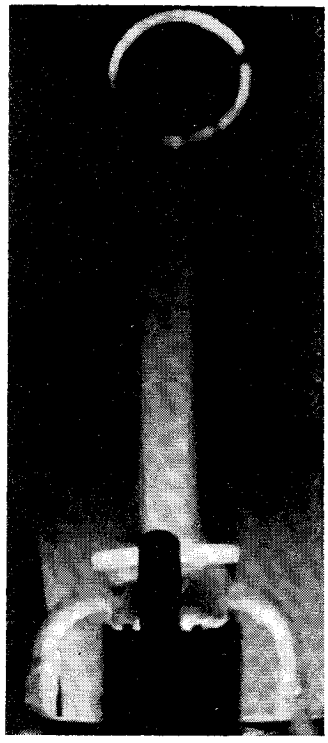

Fig. 7 Ionized lithium beam as viewed through λ5485 Å interference filter.

high-voltage mode while the conventional cathode often melted when operating in this mode. Use of a hollow cathode allowed rapid extinguishing and restarting of the arc at operating vacuums and with the lithium feed running, an operation which when attempted with the conventional cathode arc invariably led to melting of the cathode.

Operation without an Applied Magnetic Field

The hollow cathode arc was capable of operation with no applied magnetic field without damage to the arc structure. Values of the arc voltage and arc thermal efficiency obtained with no applied field are shown in Figs. 5 and 6, respectively. Visual observation of the arc head region showed that during operation with no applied field, the entire anode interior was filled with a diffuse glow, no visible jet emerged from the arc head, and the hot zone of the anode was located within its cylindrical section near the limit of the cathode extension. When the applied field was raised to several hundred gauss a definite cathode jet appeared which extended about 10 cm downstream of the anode and the anode hot zone moved downstream to the end of the anode where the cylindrical section joined the annular radiator. Increasing the magnetic field to values of about 1000 gauss, or more, resulted in the beam becoming very faint with no visible structure, although an ionized core could be observed through the λ5485 Å interference filter (Fig. 7). The visual appearance of the anode remained unchanged for all magnetic field strengths above a few hundred gauss, and indicated that the anode arc attachment remained near the downstream end of the anode cylindrical section.

IV. Beam Diagnostics

Doppler Shift Velocity Measurements

Doppler shift velocity measurements of the neutral lithium λ4602 Å line and the ionized lithium λ5485 Å line were made with a pressure scanning Fabry-Perot interferometer. The plates were coated with a broad-band dielectric coating having a reflectance of 95% or greater from 4250 Å to 7000 Å. Measurements on the λ6328 Å line emitted by a He-Ne laser showed that the interferometer had a finesse of 81.1 and a system instrumental width of 0.0164 Å. The free spectral

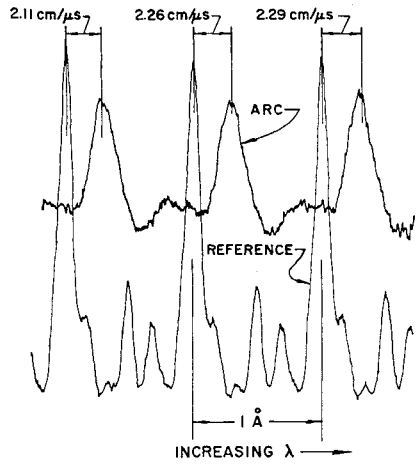

Fig. 8 Doppler shifted Fabry-Perot trace of λ5485 Å ionized lithium line.

range was 1.00 Å at λ5485 Å. This system was capable of resolving velocities as low as 1.3×10^5 cm/sec. One of the light paths was inclined at an angle of 45° to the direction of motion of the beam, and the other light path was normal to the direction of motion. A beam splitter mixed the two beams and displayed them as the shifted and unshifted lines; the Doppler shift was determined directly from the measured dispersion of the interferometer without the need for absolute wavelength measurements. For measurements of the ionized λ5485 Å line the unshifted light was obtained from a lithium hollow cathode lamp. The shifted and unshifted light beams were scanned separately in order to obtain the line profiles. The pressure scanning technique allowed each trace to begin at precisely the same wavelength. A sample of interferometer traces of the Li λ5485 Å line is shown in Fig. 8, where the trace labeled "reference" is that obtained from the hollow cathode lamp, and the trace labeled "arc" is that obtained looking at 45° to the direction of plasma motion. The velocity was determined from the usual relation

$$v = c\Delta\lambda/\lambda \cos\theta \qquad (2)$$

where $\Delta\lambda$ is the Doppler wavelength shift, λ is the wavelength of the unshifted line, c is the speed of light, and θ is the angle between the direction at which the light is observed and the direction of motion of the radiating particle.

Both the neutral and ionized particle velocities were obtained at a station 45 cm downstream of the anode face. Analysis of the neutral Li^{I}λ4602 Å line shifts obtained at arc currents between 350 and 400 amp and at input mass flows between 19 and 30 mg/sec indicated velocities in the range of 1.2 to 1.6 cm/μsec, with no apparent dependence on the applied magnetic field strength or the input mass flow rate. Velocities obtained by Doppler shift analysis of the Li^{II} λ5485 Å line are shown in Fig. 9 for arc currents beteeen 475 and 600 amp and input feed rates of 15–26 mg/sec. A point, not shown in Fig. 9, was obtained while the arc was operating in the high-voltage mode. The arc conditions were: arc current 502 amp, arc voltage 56 v, magnetic field strength 1140 gauss, input feed rate 11.8 mg/sec. The measured velocity was 2.9 cm/μsec.

Spectroscopic Temperature Measurements

As was mentioned in the previous section, the Fabry-Perot interferometer provided an accurate trace of the line profile of the ionized Li^{II}λ5485 Å line. A computer program was written which calculated the theoretical Fabry-Perot output for the fourteen component λ5485 Å line as a function of ion temperature. The program assumed pure Doppler broadening and accounted for multiple order effects. A comparison of the computed line profile for an ion temperature of 1.96 ev and an experimental profile obtained from the arc is shown in Fig. 10. Line profile measurements of the λ5485 Å line from the arc showed that the ion temperature was almost constant at about 2 ev under all arc operating conditions. Profiles of the Li^{I}λ4602 Å line were found to be Gaussian (Doppler broadened) and indicated atom temperatures of about 1.2 ev.

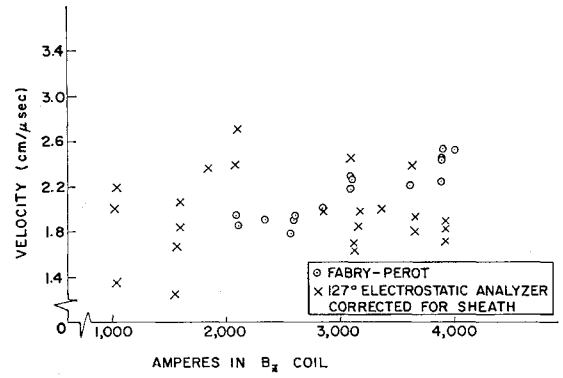

Fig. 9 Velocity vs magnetic field strength for Fabry-Perot and electrostatic energy analyzer data; magnetic field at anode face ≈ 0.485 gauss/amp.

Electrostatic Probe Measurements

Electrostatic probes similar to those described in Ref. 10 were used in an attempt to determine electron temperatures and densities. It was found that the probe temperature needed to be precisely controlled in order to avoid either shorting of the probe due to the accumulation of lithium, or failure due to the melting of the probe. Probe traces were obtained on the jet axis at a station 90 cm downstream of the anode face with the arc operating at currents between 350 and 450 amp, an arc voltage of 39 v, a lithium feed rate of 19.2 mg/sec, and an applied magnetic field of 975 gauss at the anode face. The probe current-voltage traces when analyzed in the conventional manner yielded electron temperatures of between 2.1 and 2.5 ev and electron densities between 1.4 and 1.9×10^{12}cm^{-3}. The plasma potential was determined to be between 10 and 12 v negative with respect to the anode.

Energy Analysis of Ions in the Beam

The energies and energy distribution functions for ions extracted from the beam were determined, for arc conditions similar to those reported for the Doppler shift measurements, with a 127° deflection type electrostatic analyzer. The analyzer was located on axis approximately 260 cm downstream of the arc head at the end of a 9.5-cm-diam by 118-cm-long iron tube in order to minimize magnetic field effects. While there is considerable scatter, the velocities obtained from the energy analyzer data generally support the results obtained from the Fabry-Perot Doppler shift measurements. A comparison of results is shown in Fig. 9.

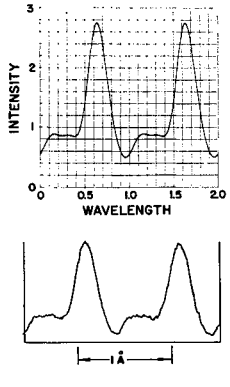

Fig. 10. Comparison of computed profile at 1.96 ev and experimental λ5485 Å line profile from the arc.

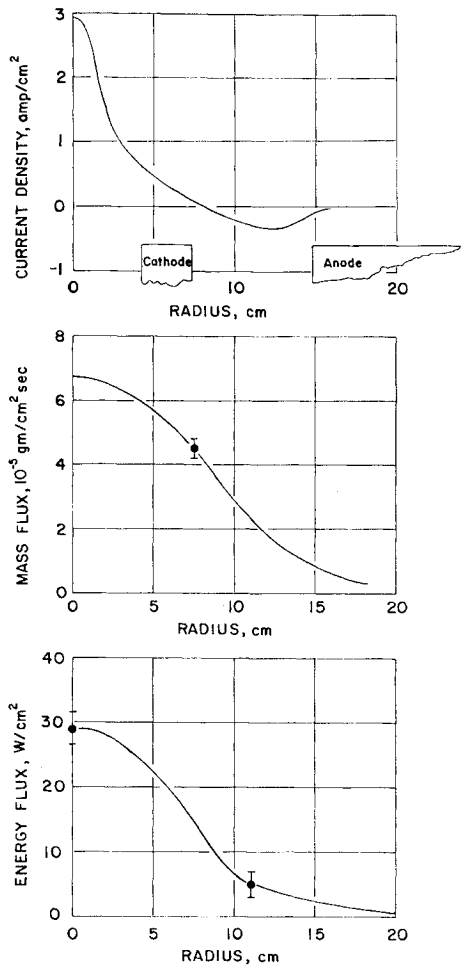

Fig. 11 Radial current density, mass flux, and energy flux profiles 90 cm downstream of the arc anode face. The downstream current as obtained from the current density profile is 135 amp, and the return current is 145 amp.

Electrostatic probe data indicated electron temperatures of about 2.3 ev 90 cm downstream of the arc head. A calculation discussed in the subsequent section on Electron Thermal Conduction shows that the electron temperature far from the arc falls very slowly. Consequently, the analyzer data shown in Fig. 11 have been corrected to account for the acceleration of ions entering the analyzer through a sheath maintained by 2.0 ev electrons.

Ion temperatures have been obtained by analysis of the energy distribution profile. Upon converting the energy distribution to a velocity distribution, and assuming a Maxwellian distribution function in the moving frame of reference, an ion temperature may be derived. Ion temperatures varied between 0.1 and 0.4 ev and showed no systematic variation with arc parameters.

Current, Mass, and Energy Distributions

It was found that when the product of arc current and applied axial magnetic field strength exceeded 10^6 gauss-amp, negative voltages with respect to ground appeared on an insulated section of the test tank beam stop. Measurements of the I-V characteristic of the potential on the insulated section showed that at the highest magnetic field strength, 3300 gauss, large currents (greater than 100 amp) could be drawn through low-impedance loads. Simultaneous with the appearance of voltage at the beam stop was a flattening of the arc voltage vs magnetic field strength characteristic, so that the arc voltage no longer increased with applied magnetic field strength (points where the product of arc current and magnetic field strength exceed 10^6 gauss-amperes are not shown in Fig. 5). These observations suggested that the region of arc currents extended downstream as far as the end of the tank when the arc was operated at very high magnetic field strengths.

A Rogowski loop with a 7.6-cm-diam opening was fabricated in order to establish the extent and magnitude of the current distribution in the arc plume. The magnitude of the axial current threading the loop was determined by electronically integrating the signal induced in the coil upon arc extinction. Radial maps of the current threading the coil were then inverted to obtain the current density distribution. The current distribution thus derived at an axial position 90 cm downstream of the anode face obtained with arc parameters of 350 amp, 55 v, and 3300 gauss at the anode face, is shown in Fig. 11 along with the projections of the cathode and anode along flux tubes originating at the arc head. The centerline current density was approximately 2.9 amp/cm², and reversed direction at a radius of 8 cm. The total axial current was 140 amp, or 0.4 of the total arc current. As indicated in Fig. 11, the region of downstream currents filled the flux tube that intersected the cathode, and the return currents filled the space out to the flux tube which returned to the inside diameter of the anode. Assuming that the electrical resistivity of the plasma plume was that corresponding to a fully ionized gas parallel to a magnetic field, at a temperature of 2.3 ev (from electrostatic probe data), $\eta = 10^{-2}$ ohm-cm. The corresponding electric field strengths to drive the measured current densities were approximately 0.01 to 0.03 v/cm.

Measurements were also made with the Rogowski loop centered on the beam axis. Signal strength was recorded as a function of the applied magnetic field strength. A summary of the results is shown in Table 1.

A time integrated profile of the mass flow in the beam was obtained by measuring the thickness of lithium deposited on a water cooled rod which extended across the vacuum tank. The profile shown in Fig. 11 was obtained by normalizing the relative mass flux so that the total lithium flow agreed with the total lithium input measured by the feed system. The error bar represents the estimated error in measuring the lithium thickness deposited on the rod.

The energy density profile shown in Fig. 11 was obtained by analysis of the temperature profile as measured by a tungsten-tungsten rhenium thermocouple. The error bars represent the estimated error introduced by uncertainties in reading the thermocouple temperature. The total measured power was 7650 w or 51% of the measured beam power. However, under the conditions at which the arc was operating, 40% of the arc current extended beyond the position at which the measurement was made.

Electron Thermal Conduction

The existence of a plasma sheath at the beam stop implied a gradient in the electron temperature along the plasma jet, since the energy required to maintain the sheath was supplied by thermal conduction in the electron gas from the arc to the beam stop.[10] The magnitude of the conduction was governed by the electron temperature at the beam stop and may be

Table 1 Centerline current through Rogowski loop

Arc current, amp	Magnetic field, gauss	Current through loop, amp
350	3150	100
350	2480	85
350	2070	65
350	1650	47
350	1240	0
350	825	0

physically visualized as that conduction necessary to supply the energy to accelerate the ionic component of the plasma through the sheath potential. It may be shown that the electron thermal conduction Φ_e is determined by the sheath potential and the ion flux, and is given by the expression[10]

$$\Phi_e = 2kT_e\dot{m}Ze/m_i \quad (3)$$

where T_e is the electron temperature adjacent to the sheath, Z is the charge on ions of mass m_i, and $\dot{m}$ is the mass flow. The thermal conduction may also be written as

$$\Phi_e = -kAdT_e/dz \quad (4)$$

where A is the conduction area, and k is the thermal conductivity. Insofar as it was observed that the jet was confined to a magnetic flux tube, the axial electron temperature distribution may be derived when 1) the mass flow is known; 2) the electron temperature near the beam stop is known; 3) the flux tube area is known at some axial position; and 4) the thermal conductivity as a function of electron temperature is known.[15] For a singly ionized gas with an electron temperature of 2 ev at the beam stop, and an input mass flow of 22 mg/sec, Φ = 1200 w. The solution for the electron temperature is shown in Fig. 12. At a station 90 cm downstream of the anode face, an electron temperature of 2.1 ev is indicated. Electrostatic probe measurements indicated an electron temperature of between 2.1 and 2.5 ev at this axial station. Computed temperatures in the arc region are about 4.5 ev.

Thrust Screen Measurements

A thrust screen was placed 83 cm downstream from the arc anode and a series of thrust measurements were made for different values of the magnetic field strength, keeping the arc current constant. The screen intercepted the entire lithium beam and the ratio of the area presented by the wires to the total screen area was 0.17. The displacement of a fiducial point on the screen was measured with a telescope and the thrust was established from the known weight of the screen and the distance from the center of mass to the point of suspension.

Thrust varied from 52 to 80 g for magnetic field strengths at the anode plane of 750 to 1900 G, respectively. Lithium velocities were derived by dividing the thrust values by the measured input Li mass flow rate through the vaporizer. The velocities were adjusted by a drag coefficient correction which took into account the gas temperature and the screen temperature. The corrected velocities ranged from 1.6 to 2.5 $\times$ 10^6 cm/sec.

Figure 13 shows that the thrust on the screen increased as B_z increased. The Rogowski coil measurements discussed previously showed that substantial currents extended downstream of the thrust screen location and that the fraction of the arc current which extended downstream of the screen increased with increasing B_z. It was probable, therefore, that thrust was being imparted to the gas downstream of the screen measurement. Li ion velocities determined simultaneously from Doppler shift measurements at a station 48 cm upstream of the screen showed ion velocities of approximately 0.85 the screen data, in agreement with the supposition of continuous acceleration of plasma throughout the region of current extension.

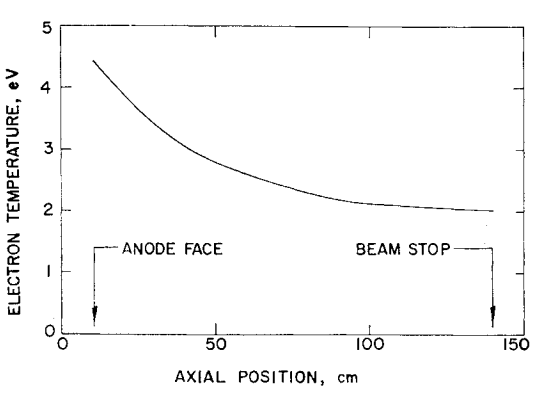

Fig. 12 Electron temperature as a function of axial position for a singly ionized beam with an electron temperature of 2 ev at the beam-stop and an input mass flow of 22 mg/sec.

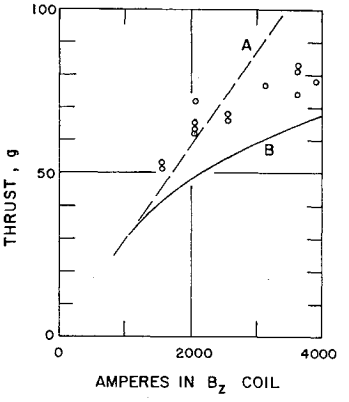

Fig. 13 Thrust vs current in magnetic field coils; magnetic field at anode face ≈ 0.485 gauss/amp. The points are measured values. The curve *A* is calculated from Eq. (16). The curve *B* is reduced from curve *A* by (*1-f*), where *f* is the fraction of the total current extending downstream of the thrust screen (see Table 1).

The thrust efficiency, defined as $(F^2/2\dot{m})/P_{\text{arc}}$, where F is the thrust and $\dot{m}$ the mass flow rate, and P_{arc} is the electrical power input to the arc, varied from 0.28 to 0.48 for magnetic field strengths at the anode face of 750 to 1900 G, respectively.

The power in a beam of singly charged ions is given by[10]

$$P_{\text{beam}} = (\dot{m}/m_i)(\tfrac{3}{2}kT_i + 2kT_e + eV_s + e\phi + m_iL) + F^2/2\dot{m} \quad (5)$$

where V_s and ϕ are the appropriate sheath and ionization potentials, F is the thrust, and L is the energy of condensation. The total power in the beam as derived from Eq. (5) was generally about 1.15 times the calorimetrically measured power. It was found that a simple adjustment of the mass flow rate, either upward or downward, would not correct the discrepancy, which required instead a reduction in the magnitude of the coefficient of $\dot{m}$ in the first term of Eq. (5) from 16 ev to 12 ev, or in the magnitude of the thrust by about 12%, or some combination of both.

V. Discussion

The very large value of the Hall parameter which characterizes these experiments causes the electronic component of the arc current to run downstream along flux tubes, seeking regions of lower Hall coefficient. The Hall parameter, defined in terms of the electrical resistivity η by $\omega/\nu = B/ne\eta$, is between 30 and 100 at the position 90 cm downstream of the arc head where the electron temperature and density were measured with probes. ω/ν increases towards the arc head since $B/n \simeq$ const., and the resistivity decreases as the electron temperature increases. For example, Fig. 12 shows that the electron temperature must be approximately 4 ev in the vicinity of the arc head, and $\omega/\nu \simeq 100$ to 300.

The azimuthal current density due to electrons circulating with the $\bar{E} \times \bar{B}$ drift is neE/B, or approximately 20 amp/cm^2 for the conditions of the arc. The radial current density is then 20 ν/ω amp/cm^2, or somewhat less than 0.1 amp/cm^2. In the same regions ions are accelerating in the azimuthal direction and reduce the net plasma current. An estimate of the net current may be made by observing that the radial electromagnetic forces are balanced by the centrifugal terms. Then, writing the radial equation

$$\rho v_\theta^2/r = ne\,(v_e - v_i)\,B = j_\theta B_z \quad (6)$$

where v_i is the rotational velocity of the ions, and $v_e \simeq v_D$, where v_D is the $\bar{E} \times \bar{B}$ drift, we find that

$$v_i^2 + v_g v_i - v_g v_D = 0 \tag{7}$$

$v_g = \mathrm{Ber}/M$, and is the velocity of ions of mass M gyrating with radius r in a magnetic field of strength B. Estimates of the magnitude of the ratio v_g/v_D show that for these arc conditions $1 < v_g/v_D < 10$. The corresponding range of values for v_i/v_D is $0.6 < v_i/v_D < 0.9$. The 20 amp/cm^2 of circulating electrons are offset by some 15 amp/cm^2 of ion drift, for a net current in the azimuthal direction of approximately 5 amp/cm^2.

The electromagnetic force terms which contribute to plasma acceleration have been described many places. A discussion of the $\bar{\jmath} \times \bar{B}$ terms will be attempted here with the possible range of values for our arc operating conditions. As a set of nominal values we take: $I_{\mathrm{arc}} = 350$ A, $V_{\mathrm{arc}} = 58$ v, $B_{z_0} = 2000$ G at Magnet Plane, $B_{z_A} = 1500$ G at Anode Face, $\dot{m} = 25$ mg/sec Li corresponding to 340 A Li$^+$, $r_A = 1.9$ cm, $r_C = 0.55$ cm.

Forces due to the interaction of the arc currents with B_θ are the self field forces $j_z B_\theta$ and $j_r B_\theta$. $j_r B_\theta$ is axial; $j_z B_\theta$ is radial and contributes to the axial force through the plasma pressure. The magnitudes of these terms for the nominal arc conditions are

$$j_r B_\theta: (\mu_0/4\pi) I^2 [\tfrac{1}{4} + \ln(r_a/r_c)] = 1.85 \text{ g} \tag{8}$$

$$j_z B_\theta: (\mu_0/4\pi) I^2 (\tfrac{1}{2}) = 0.63 \text{ g}$$

The application of an external magnetic field to the coaxial MPD arc introduces the additional terms $j_r B_z$, $j_z B_r$, $j_\theta B_z$, and $j_\theta B_r$ into the expansion of $\bar{\jmath} \times \bar{B}$. The force terms tending to put the plasma into rotation are $j_r B_z$ and $j_z B_r$. As is the case with the self-field forces, the upper limit of these terms may be evaluated without specific knowledge of the current distributions. The actual location of the current carrying region and the spatial distribution of the forces producing plasma rotation do not change the value of the torque on the plasma.

The torque may be established by integrating $j_r B_z$ radially in the plane of symmetry of the magnet, where $B_r = 0$. The value of j_r is that corresponding to the total arc current; and the limits of radial integration are determined by projecting the radial position of arc attachment on the anode and cathode back to the magnet plane along flux tubes. The torque on the plasma is

$$L = \tfrac{1}{2} BI (R_a^2 - R_c^2) = d/dt(i\omega) \tag{9}$$

where B and I are the magnetic field and arc current, R_a and R_c are the anode and cathode radii projected to the plane of the magnet and i is the moment of inertia of the rotating plasma. When the plasma rotates as a solid object, i.e., $v_\theta = \omega r$, the time rate of change of kinetic energy in rotation is

$$P = d/dt\, \tfrac{1}{2} i\omega^2 = \dot{m}\omega^2 (R_a^2 + R_c^2)/4 \tag{10}$$

Conversion of the rotational energy to directed flow results in a thrust T

$$T^2 = \tfrac{1}{2} \dot{m}^2 \omega^2 (R_a^2 + R_c^2) \tag{11}$$

The torque is $\dot{m} (R_a^2 + R_c^2)\, \omega/2$. Substituting for $\dot{m}\omega$, and the torque,

$$T \simeq (2^{1/2}/2) BIR_a [1 - \tfrac{3}{2}(R_c/R_a)^2] \tag{12}$$

The axial thrust due to conversion of rotational forces does not exceed 71 g for the nominal arc operating conditions.

It has been assumed without discussion that rotational energy and momentum are converted to axial thrust through expansion in the magnetic nozzle. An insight into this process may be obtained from an examination of the motion of an element of mass which is confined to a flux tube and expands with the flux tube. The angular momentum residing in the element of mass δm is $P_\theta = \delta m\, v_\theta\, r$. Since $\partial p_\theta/\partial z = 0$, we have

$$\delta m [r\, \partial v_\theta/\partial z + v_\theta \partial r/\partial z] = 0 \tag{13}$$

At the same place we have

$$\partial r/\partial z = B_r/B_z \tag{14}$$

The total energy $\frac{1}{2}\, \delta m\, (v_\theta^2 + v_z^2)$ is conserved. Differentiating with respect to z

$$\delta m (v_\theta \partial v_\theta/\partial z + v_z\, \partial v_z/\partial z) = 0 \tag{15}$$

The axial force on the element of mass may be expressed as $\partial W_z/\partial z$ where W_z is the axial energy of the element of mass δm. Then

$$F_z = \partial W_z/\partial z = \delta m\, v_z\, \partial v_z/\partial z \tag{16}$$

and substitution from Eqs. (15) and (13) yields

$$F_z = \delta m (v_\theta^2/r) \partial r/\partial z \tag{17}$$

The force per unit volume is

$$f_z = (\rho v_\theta^2/r) \partial r/\partial z \tag{18}$$

As a condition of radial confinement we have from Eq. (6) that $\rho\, v_\theta^2/r = j_\theta B_z$. Also, $\partial r/\partial z = B_r/B_z$, so that Eq. (18) becomes

$$f_z = j_\theta B_r \tag{19}$$

We see, therefore, that the axial force $j_\theta B_r$ allows a rotating plasma confined to a magnetic field to expand or contract with the flux tubes with conservation of the rotational angular momentum. Boyer, et al.[17] show that the condition for magnetic containment leads to the following relationship between V_{rot} and the magnetic field strength at the outer electrode

$$(1 + m_e/m_i)[V_{\mathrm{rot}}/\ln(R_A/R_C)]^2 = B_A{}^4 R_A{}^2 R_C{}^2/ [2\mu_0 n m_i (R_A{}^2 - R_C{}^2)]$$

Our case of 1500 G at the anode and $V_{\mathrm{rot}} = 35$ v corresponds to a maximum contained particle density of approximately 6×10^{14} cm^{-3}.

An alternate description of the azimuthal currents may be obtained from an examination of the electron and ion drifts. The principal drifts arise because of the crossed $\bar{E}$ and $\bar{B}$ fields, and from the centrifugal force. The general expression for the drift velocity is

$$V_D = \bar{f} \times \bar{B}/(e|B|^2) \tag{20}$$

The E-field drift has for the force term eE so that ions and electrons drift in the same direction and tend to produce no net current as v_{θ_i} approaches v_{θ_e}. The centrifugal drift, however, is in different directions for particles of different charge and always results in a net current. Summarizing, for singly charged particles

$$\bar{\jmath}_\theta = ne[-v_c \pm (v_{E_i} - v_{E_e})]\hat{\theta} \tag{21}$$

where v_c is the centrifugal drift velocity and v_E is the drift velocity due to the electric field. The plus sign occurs with normal polarity (center electrode negative) and the minus sign occurs with reverse polarity. $\bar{B}$ has components in the positive r and z directions.

The importance of the sense of the various azimuthal drifts has been demonstrated by reversing the polarity of the arc. Coaxial MPD arcs operated with the center electrode negative produce a well defined plasma plume. When the center electrode is positive there is no emergent plume and nearly all of the arc power is dissipated in the electrodes.[10] Qualitatively the arc performs better when the ionic current due to the centrifugal drift is in the same direction as the current

due to electrons drifting in the $\bar{E} \times \bar{B}$ direction. Because of the ion inertia the electron drifts in the $\bar{E} \times \bar{B}$ direction are the first to develop and it appears to be necessary for the successful generation of the arc that the $\bar{\jmath} \times \bar{B}$ forces from the electron drift be in such a direction as to force the gas off of the outer electrode.

The Hall acceleration term $j_\theta B_r$ is in fact equivalent to the steady-state expansion along field lines of a rotating fluid confined to a magnetic flux tube. As a consequence, the thrust developed in a MPD arc by $\bar{\jmath} \times \bar{B}$ forces is given by the sum of the self field forces [Eq. (8)] and the conversion of rotation into directed flow [Eq. (12)]. Further considerations of the rotation are described in the Appendix, where conclusions concerning the efficiency and mass flow rate are derived. These may be summarized by observing that the analysis leads to a thrust efficiency of 0.5§ (excluding thermal and self-field thrusts) and that the mass flow rate should be $> m_i I/2e$ where I is the arc current.

The rotational analysis shows that part of the arc voltage is due to a back emf developed as the fluid rotates in the magnetic field. The back emf should be functionally related to the arc parameters according to

$$V_{\text{rot}} = v_\theta BR \tag{22}$$

However, the azimuthal velocity should be linearly related to the strength of the applied magnetic field, so that Eq. (22) becomes

$$V_{\text{rot}} = B^2 I R^2/(2\dot{m}) \tag{22'}$$

It is experimentally observed that the arc voltage tends to favor two modes, a low-voltage mode in which the voltage increases only linearly with the strength of the applied magnetic field, and a high-voltage mode in which a B^2 dependence is indicated.[14] Quantitative agreement with the magnitude of V_{rot} in the low voltage mode is obtained for a wide variety of working fluids when the Alfvén critical velocity is substituted for $v_\theta[v_{cr} = (2e\phi_i/m_i)^{1/2}]$, where ϕ is the first ionization potential of the working fluid. Since the Alfvén velocity is judged to be significant only in regions of partial ionization it appears that the arc voltage is governed in the low-voltage mode by rotation where ionization occurs. As the feed rate is reduced the arc voltage increases, and tends to show a square law dependence on B, in agreement with Eq. (22'). At the same time, the power loss to the electrodes increases, and it is not always possible to predict for a given arc whether operation in the high voltage mode can occur without electrode destruction.

A space charge field always accompanies $\bar{\jmath} \times \bar{B}$ acceleration of plasma if electrons carry a large fraction of the current and the collisional rate of momentum exchange from electrons to ions is inadequate to transmit the force. Electrons experience the $\bar{\jmath} \times \bar{B}$ force and tend to move away from the ions. If the geometry is suitable, as for example, it is in a parallel electrode accelerator, a strong axial electric field is established by the separation of charge which transfers the force to the ions. The $\bar{\jmath} \times \bar{B}$ force in MPD arcs is predominantly azimuthal, and there is no opportunity for charge separation as long as the arc is azimuthally symmetric. Since, however, the electrons carry some of the current, and the collisional transfer rate is very slow for the plasma densities involved, it becomes necessary for an electric field of strength

$$E_\theta = j_r B_z/(n_e e) \tag{23}$$

to accelerate the ions azimuthally. In order to allow the existence of E_θ the arc symmetry must be destroyed, as has been demonstrated in nearly all MPD experiments. It appears, then, that the results of pulsed experiments on plasma acceleration[16] may have relevance to the azimuthal acceleration of plasma in MPD arcs.

§ Recent numerical calculations indicate that if acceleration takes place in a diverging magnetic field, thrust efficiencies greater than 0.5 may be obtained under some conditions of downstream current extension.

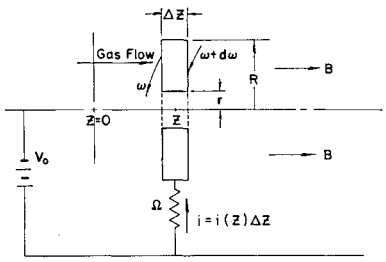

Fig. 14 Schematic of rotating plasma motor.

VI. Conclusions

The electromagnetic acceleration of lithium ions is well established by these experiments. The plasma plume is fully ionized and the axial energy of the lithium is too great to be accounted for by the expansion of a heated gas. However, several unexpected features of the arc operation have emerged from the experiments. Principal among these is the downstream extension of the arc currents; associated with this phenomenon appears to be the fact that current streamlines follow the magnetic flux tubes into regions of remarkably small magnetic field—fields as low as 20 G. Another feature which appears is the fact that the thermal efficiency, defined as $P_{\text{beam}}/\text{VI}$, is virtually independent of all arc parameters (except at very low B_z and zero B_z), and assumes the value 0.70 ± 0.03.

Appendix

The steady-state problem which leads to plasma rotation in a MPD accelerator has many features in common with the startup of a homo-polar motor.

It is well known that, aside from the starting transient, a motor, whether homo-polar or otherwise, approaches unit efficiency as the motor resistive impedance goes to zero. Insofar as the plasma motor is imagined to be a steady-state device, is it not likely that it, in analogy with the steady motor case, is capable of unit efficiency? We examine whether this is the case by consideration of Fig. 14.

Conducting gas which constitutes the rotor enters from the left. There are no axial forces in the problem considered so that the axial flow remains uniform at velocity v_z. There is a resistor Ω in the circuit so that the sum of the back emf at the position Z where the angular velocity is ω (assumed to correspond to rigid body rotation) and the drop through the resistor, $i\Omega$, is equal to the applied voltage V_o. We let the density be defined by $\rho = \rho_o f(r)$, where $f(r)$ is an arbitrary function, and find the following expressions to hold.
Increase in angular momentum across ΔZ:

$$\Delta P(Z) = 2\pi\rho_o \left[\int_r^R r^3 f(r)dr\right] d\omega \Delta Z \tag{A1}$$

Increase in energy in rotation across ΔZ:

$$\Delta W(Z) = 2\pi\rho_o \omega(Z) \left[\int_r^R r^3 f(r)dr\right] d\omega \Delta Z \tag{A2}$$

Torque on the element:

$$L(Z) = \tfrac{1}{2} i(Z) B(R^2 - r^2)\Delta Z \tag{A3}$$

Ohm's Law

$$V_o = \tfrac{1}{2}\omega(Z)B(R^2 - r^2) + i(Z)\Omega(Z) \tag{A4}$$

Since

$$\dot{m} = 2\pi v_Z \rho_o \int_r^R rf(r)dr$$

we have that the time for an element of fluid to traverse a distance dz is $dz/v_z = dt$, or

$$dt = (2\pi\rho_o/\dot{m}) \int_r^R rf(r)dr$$

Then,
Rate of increase of angular momentum:

$$L(Z) = dP(Z)/dt = \dot{m} \left[\int_r^R r^2 f(r)dr\right] d\omega \Big/ \int_r^R rf(r)dr \tag{A5}$$

Rate of increase in energy in rotation:

$$dW(Z)/dt = L(Z)\omega(Z) = \dot{m}\omega\Big[\int_r^R r^2 f(r)dr\Big]d\omega \Big/ \int_r^R rf(r)dr \tag{A6}$$

Letting the axial distribution of current be described as $i(Z) = i_o f(Z)$ where $f(Z)$ is an arbitrary function, the total current I is

$$\int_o^{Z_f} i_o f(Z)dz$$

where Z_f is the limit of downstream current extension. Then, solving for the angular velocity as a function of axial position

$$\omega(Z) = Bi_o(R^2 - r^2) \int_r^R rf(r)dr \int_o^Z f(Z)dZ \Big/ \left(2\dot{m} \int_r^R r^3 f(r)dr\right) \tag{A7}$$

The kinetic power in the fluid W_k is

$$\int_o^{Z_f} \dot{W}(z)dz$$

or

$$W_k = B^2 i_o^2 (R^2 - r^2)^2 \int_r^R rf(r) \int_o^{Z_f} f(Z) \times \Big[\int_o^Z f(Z')dZ'\Big]dZ \Big/ \left(4\dot{m} \int_r^R r^3 f(r)dr\right) \tag{A8}$$

Solving for V_o

$$V_o = B^2 I(R^2 - r^2)^2 \int_r^R rf(r)dr \Big/ \left(4\dot{m} \int_r^R r^3 f(r)dr\right) \tag{A9}$$

The efficiency η defined as the ratio of the kinetic power to the total input power is

$$\eta = W_k/(IV_o) = \int_o^{Z_f} f(Z)\Big[\int_o^Z f(Z')dZ'\Big]dZ \Big/ \left(\int_o^{Z_f} f(Z)dZ\right)^2$$

It may be shown that for all forms of $f(Z)$

$$2 \int_o^{Z_f} f(Z)\Big[\int_o^{Z_f} f(Z')dZ'\Big]dZ \equiv \Big[\int_o^{Z_f} f(Z)dZ\Big]^2$$

Thus $\eta \equiv \frac{1}{2}$.

An expression relating current and mass flow may be obtained from the preceding relationships when it is assumed that the kinetic energy of ions is not greater than that gained by falling through the applied voltage. This assumption is consistent with the collisionless character of the flow. The kinetic power obtained by a stream of ions having an energy some fraction β of the applied voltage is $\dot{m}Ze\beta V_o/m_i$. Equating this expression to the kinetic power given by Eq. (A8), one obtains after some manipulation that

$$\dot{m}Ze/m_i = \tfrac{1}{2}I/\beta \tag{A10}$$

This analysis shows that the efficiency of conversion of electrical power directly into rotational kinetic power is accomplished with an efficiency of $\frac{1}{2}$, and that an equal amount of power is dissipated in joule losses. The resistors Ω are present in order to allow Ohm's Law to be obeyed at all places where current flows and the rotational back emf is not equal to the applied voltage. In reality, they are composed of sheath drops and ohmic resistance in the plasma. The energy which is deposited by joule heating of the plasma may be recovered in part by expansion, but the efficiency of conversion of electrical power directly into kinetic power is $\frac{1}{2}$ for the type of plasma motor discussed. Various realistic losses in viscous flow, and conversion from rotational to axial flow will reduce the efficiency somewhat more.

References

[1] Kruelle, G., "Characteristics and Local Analysis of MPD Thruster Operation," AIAA Paper 67-672, Colorado Springs, Colo., 1967.

[2] Cann, G. L., Harder, R. L., and Nelson, S. T., "Experimental Performance of the Alpha Thruster," AIAA Paper 67-687, Colorado Springs, Colo., 1967.

[3] John, R. R., Bennett, S., and Conners, J. F., "Experimental Performance of a High Specific Impulse Arc Jet Engine," *Astronautica Acta*, Vol. 11, No. 2, 1965, pp. 97–103.

[4] Burlock, J. et al., "Measurements of Velocities and Acceleration Mechanisms for Coaxial Hall Accelerators," *AIAA Journal*, Vol. 5, No. 3, March 1967, pp. 558–561.

[5] Patrick, R. M. and Schneiderman, A. M., "Performance Characteristics of a Magnetic Annular Arc," *AIAA Journal*, Vol. 4, No. 2, Feb. 1966, pp. 283–290.

[6] Ducati, A. C., Giannini, G. M., and Muehlberger, E., "Experimental Results in High-Specific-Impulse Thermo-Ionic Acceleration," *AIAA Journal*, Vol. 2, No. 8, Aug. 1964, pp. 1452–1454.

[7] Malliaris, A. C., "Oscillations in an MPD Accelerator," *AIAA Journal*, Vol. 6, No. 8, Aug. 1968, pp. 1575–1577.

[8] Connolly, D. J. et al., "Low Environmental Pressure MPD Arc Tests," *AIAA Journal*, Vol. 6, No. 7, July 1968, pp. 1271–1276.

[9] Larson, A. V., "Experiments on Current Rotations in an MPD Engine," *AIAA Journal*, Vol. 6, No. 6, June 1968, pp. 1001–1006.

[10] Blackstock, A. W. et al., "A Cesium MHD Arc Jet," *Journal of Applied Physics*, Vol. 39, No. 7, June 1968, pp. 3201–3209.

[11] Nerheim, N. M. and Kelly, A. J., "A Critical Review of the State-of-the-Art of the MPD Thrustor," AIAA Paper 67-688, Colorado Springs, Colo., 1967.

[12] Grover, G. M., Cotter, T. P., and Erickson, G. F., "Structures of Very High Thermal Conductance," *Journal of Applied Physics*, Vol. 35, No. 6, June 1964, pp. 1990–1991.

[13] Alfvén, H., "Collision Between a Nonionized Gas and a Magnetized Plasma," *Reviews of Modern Physics*, Vol. 32, No. 4, Oct. 1960, pp. 710–713.

[14] Fradkin, D. B., Blackstock, A. W., and Roehling, D. J., "Voltage Modes of a Lithium-Fueled MPD Arc Jet," *Proceedings of Ninth Symposium on Engineering Aspects of Magnetohydrodynamics*, AIAA, ASME, and IEEE, Tullahoma, Tenn., April 3–5, 1968, pp. 27–28.

[15] Spitzer, L., Jr., *Physics of Fully Ionized Gases*, Interscience, New York, 1956.

[16] Lovberg, R. H., "Investigation of Current-Sheet Microstructure," *AIAA Journal*, Vol. 4, No. 7, July 1966, pp. 1215–1222.

[17] Boyer, K. et al., "Theoretical and Experimental Discussion of Ixion, a Possible Thermonuclear Device," *Proceedings of the Second United Nations International Conference on the Peaceful Uses of Atomic Energy*, Vol. 31, 1958, pp. 319–324.